Sensors & Actuators: B. Chemical 332 (2021) 129504

Contents lists available at ScienceDirect

Sensors and Actuators: B. Chemical

journal homepage: www.elsevier.com/locate/snb

Integrated microfluidic helium discharge photoionization detectors

Maxwell Wei-Hao Li [a,b,c,1], Abhishek Ghosh [a,b,1], Ruchi Sharma [a,b], Hongbo Zhu [a,b], Xudong Fan [a,b,*]

[a] Department of Biomedical Engineering, University of Michigan, Ann Arbor, MI 48109, USA
[b] Center for Wireless Integrated MicroSensing and Systems (WIMS^2), University of Michigan, Ann Arbor, MI 48109, USA
[c] Department of Electrical Engineering and Computer Science, University of Michigan, Ann Arbor, MI 48109, USA

ARTICLE INFO

Keywords:
Photoionization detector
Universal gas detection
Volatile organic compounds
Portable gas chromatography
Helium dielectric barrier discharge plasma

ABSTRACT

Helium discharge photoionization detectors (HDPIDs) have been of increasing importance for detection of highly volatile compounds in gas chromatography (GC) and portable gas monitoring systems. The high ionization energy of these detectors (13.5–17.5 eV) allows for detection of virtually all compounds of interest, offering a distinct advantage compared to conventional PIDs, which can only detect compounds with ionization potentials below 10.6 (or 11.7, if using argon) eV. However, many current designs are bulky, power intensive, or helium intensive, restricting their usage to benchtop laboratory use. We recently developed a miniaturized HDPID that has low power and helium consumption, and small footprint. While offering suitable performance for portable GC applications, this design relies on hand assembly of silicon and Pyrex glass pieces, reducing fabrication yield, robustness, and repeatability. The current work improves on this prior device using an integrated, microfabricated μHDPID chip along with in-house designed plasma excitation and readout circuits. The μHDPID is characterized using permanent gases, light hydrocarbons, and formaldehyde, achieving low detection limits better than 10 pg, high linearity, rapid response time, short warm-up time, and high repeatability among devices. This integrated on-chip gas sensor offers advantages in ease of fabrication, yield and robustness, and repeatability. Therefore, it can be broadly used in portable GC for various applications.

1. Introduction

Plasma-based photoionization detectors (PIDs) are commonly used for detection of highly volatile compounds in gas monitoring and analysis applications [1–8]. Their high sensitivity, large dynamic range, low cost, fast response times, and small size make them especially useful for portable gas analysis, such as in portable gas chromatography (GC) systems [3–7,9–11]. Typical PIDs utilize sealed lamps (made of ultraviolet transparent materials such as LiF or MgF_2) containing noble or permanent gases (e.g., xenon, krypton, and argon) to excite plasma and thereby generate photons ranging from 9.6–11.7 eV. While highly suitable for many GC applications, the limited photon energy (< 11.7 eV) generated by regular PIDs prevents detection of chemicals with high ionization energies, limiting the scope of portable GC to a restricted set of compounds.

More recently, research has been directed toward development of helium discharge PIDs (HDPIDs), which use helium flows to generate plasma that emits photons ranging from 13.5–17.5 eV [12–35]. In comparison with regular 10.6 eV or 11.7 eV PIDs, HDPIDs have been shown to efficiently ionize and detect virtually all volatile chemicals of interest [13,16,17,23,24,31], including those with ionization potentials close to or above 11.7 eV (e.g., methane and carbon tetrachloride). This provides a significant advantage over conventional lamp-based PIDs, which cannot detect high ionization potential compounds such as formaldehyde or methane. In particular, dielectric barrier discharge (DBD) plasma generation using high voltage (~10s-100 s kV) and high frequency (up to several MHz) along with usage of dielectric materials to protect the electrode surface from the discharge plasma has allowed for highly homogeneous discharge and long electrode lifetime [20,21,30,31,33,13–35]. These improve device performance (especially noise) and durability. Other methods such as pulsed or direct current discharge are also commonly applied for plasma generation [12,13,15–19,22,23,25,26,28,29,36], where either pulsed or continuous high voltages are used to generate helium ions. In the case of direct current discharge plasmas,

* Corresponding author at: Department of Biomedical Engineering, University of Michigan, Ann Arbor, MI 48109, USA.
E-mail address: xsfan@umich.edu (X. Fan).
[1] Equal contribution.

https://doi.org/10.1016/j.snb.2021.129504
Received 20 October 2020; Received in revised form 20 December 2020; Accepted 8 January 2021
Available online 19 January 2021

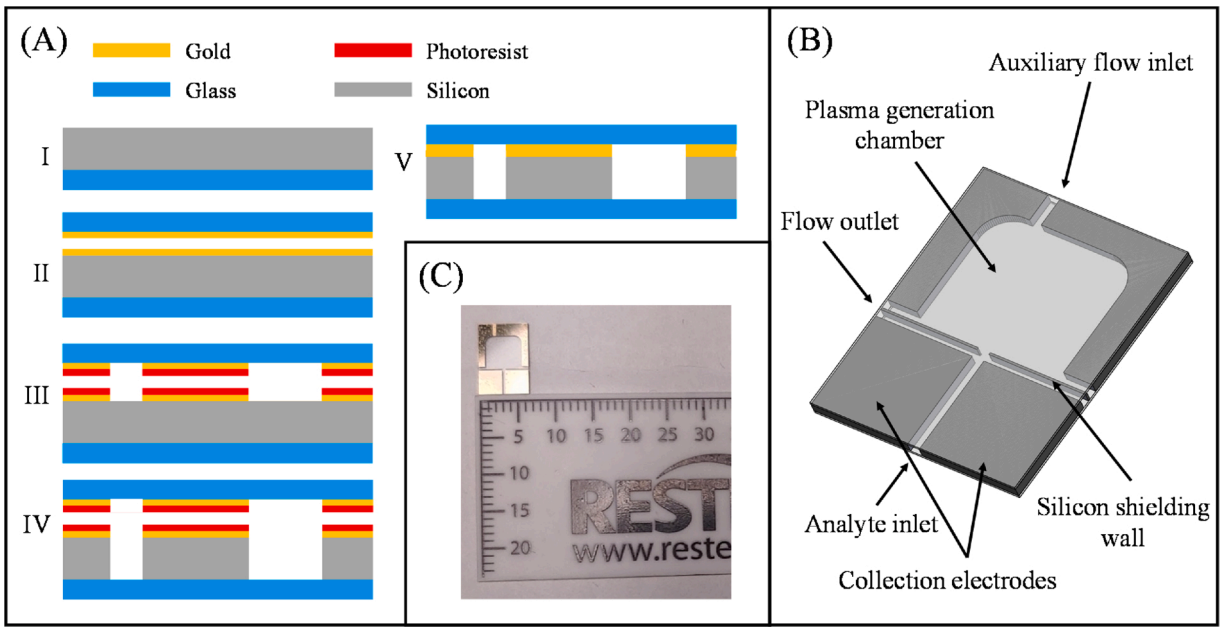

Fig. 1. (A) μHDPID fabrication procedure. I. Anodic bonding between glass and silicon. II. Gold deposition on bonded wafer and fresh glass wafer. III. Patterning and gold etching. IV. DRIE to etch channels in silicon. V. Photoresist stripping and eutectic bonding. (B) SolidWorks® schematic of single μHDPID chip. (C) Photograph of μHD-PID (eutectically-bonded side facing up). The final chip was 10 mm x 7 mm x 0.75 mm (L x W x H) in size. Detailed chip dimensions are provided in Figure S1.

most excitation voltages are in the range of a few hundred V [15,25,26,33], while pulsed discharge plasmas utilize pulses on the ms (occasionally μs) timescale to excite the plasma [13,17,16–19,28,29,33,36]. However, in pulsed or direct current discharge, the lack of dielectric protecting the electrode surface (present in DBD) means that high energy ions bombarding the electrode material degrade the detector over time, necessitating frequent maintenance or replacement. In general, these varying methods have allowed for development of non-destructive detectors with high sensitivity down to a few picograms [13,19,22,23,25], achieving near or subsecond peak widths [13,18,22,23,25], and linear dynamic range up to 7 decades [35], which allows for competitive performance compared to other GC detectors like flame ionization detectors and thermal conductivity detectors.

While the HDPID's high energy makes it a nearly universal detector for gas analysis, in contrast to regular PIDs, most HDPIDs are not applicable to portable GC systems. In an optimized device, the power consumption of the detector itself can be reduced to as low as 1.4 mW [23], but the total system power consumption (measured at the supply) is typically high (up to 12.5 W) [17,27,30,33]. Likewise, the auxiliary helium flow may be reduced to as low as 1 mL/min with specialized designs [23,25], but most systems are helium intensive (up to 300 mL/min) [18,27,31,35], which is prohibitive for portable systems. Additionally, most HDPIDs are bulky in size and weight (comparable to typical flame ionization detector) [18,19,24,27,31,35], especially considering necessary auxiliary system components, such as plasma generation supplies, transformers, and readout circuits. For a portable HDPID system, low power and helium consumption, small footprint, and device robustness are all important characteristics for practical use.

Zhu et al. previously addressed several of these issues by developing a hand-assembled microfluidic HDPID featuring low power consumption (<400 mW), helium consumption (5.8 mL/min), and small size and weight (15 mm x 10 mm x 0.7 mm, 0.25 g), while maintaining picogram-level sensitivity and a dynamic range of over 4 orders of magnitude [21]. The characteristics and performance of this HDPID are well suited for portable GC development, but the hand-crafted nature of this device greatly reduces fabrication repeatability, robustness, and scalability; such an assembly process cannot be automated for mass-scale production. When factoring in variability due to human assembly, device sensitivity, bias voltage, optimal auxiliary flow, optimal carrier gas flow, and response time become variables as well, meaning that two such HDPIDs may require quite different parameters in order to obtain similar results. Thus, extensive optimization was required for even a single device to operate well.

This paper presents a method for repeatable, robust microfabrication of integrated microfluidic μHDPIDs along with in-house designed plasma excitation and readout circuits. Compared to the previous hand-assembled design, this work allows for high yield and low variability between devices, alleviating the need for extensive optimization on each individual chip. The additional use of in-house designed circuits and miniature power supply enables truly portable operation for *in situ* experiments (as compared to [21], which used external power supplies and readout circuits). Further comparison between the current work and other HDPIDs is provided in Table S1. The entire system (including power supply, circuit, and μHDPID chip) can be contained within a copper mesh shield of dimensions 11.5 cm × 9 cm × 5 cm. The μHDPID fabrication process and device characterization are detailed herein along with analysis of permanent gases, light hydrocarbons, and formaldehyde, which have applicability for field analysis by portable GC. Detection limits on the order of or better than 10 pg are shown to be achievable for various volatile compounds, including those with ionization energies above 10.6 eV and even 11.7 eV. Permanent gases having high ionization potential are also analyzed, with detection limits better than 20 pg. The μHDPID is additionally shown to have high linearity for injections ranging from 50 pg to 10 ng, rapid response time (~100 ms), short warm-up time (within 15 s), and high repeatability among devices.

2. Materials

Analytical standard grade pentane, heptane, benzene, toluene, dichloromethane, chloroform, carbon tetrachloride, acetone, tetrahydrofuran, ethyl acetate, pyridine, isopropanol, methanol, formic acid, formaldehyde, and acetaldehyde were purchased from Sigma-Aldrich (St. Louis, MO). Oxygen, argon, carbon dioxide, methane, ethane, hydrogen, and nitrogen were purchased from Gasco (Oldsmar, FL). Argon was purchased from Cryogenic Gases (Ann Arbor, MI). Hysol®

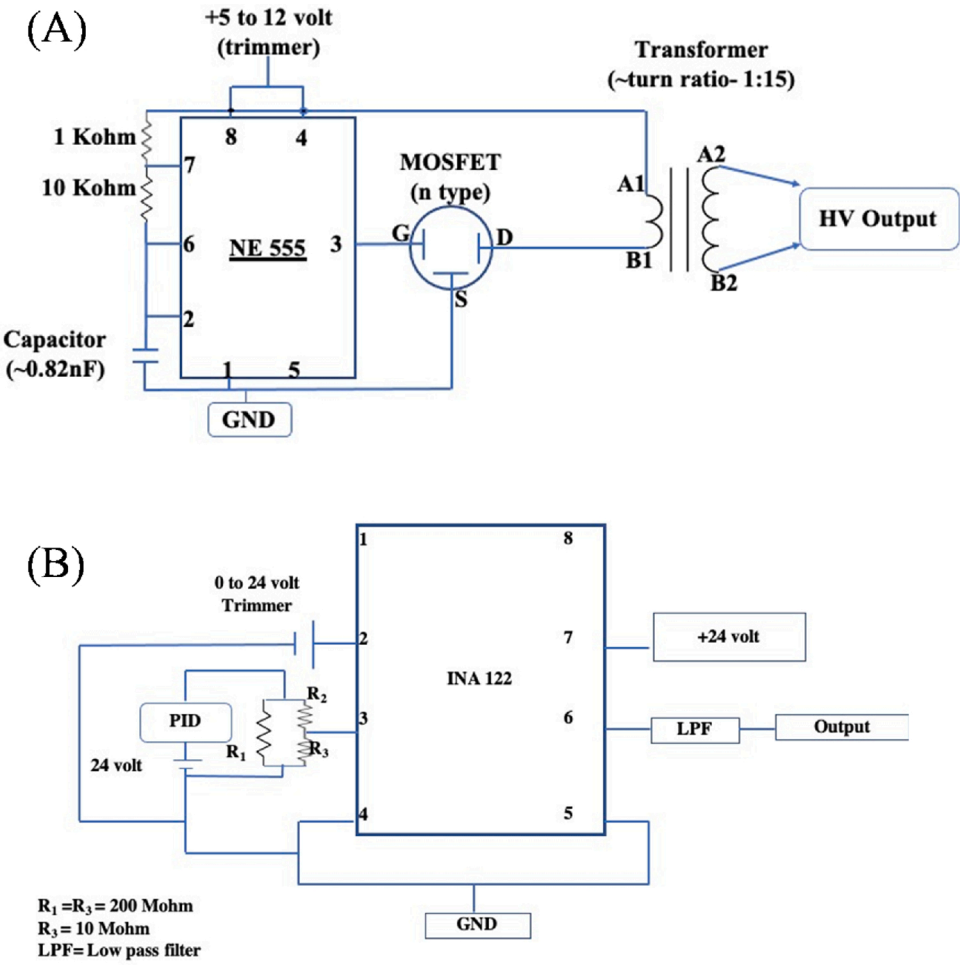

Fig. 2. (A) Plasma generation circuit. The HV output is an AC signal with an amplitude of ~0.9 kV and a frequency of 83.6 kHz. (B) Amplification circuit. The supply voltage is 24 VDC. The collection electrodes are biased with 24 V. The voltage is read out through the network of R_1, R_2, and R_3, which have an equivalent resistance of ~102 MΩ. The low pass filter cutoff frequency is 1.5 Hz. PID – photoionization detector.

1C™ Epoxy was purchased from Ellsworth Adhesive (Germantown, WI). Deactivated fused silica tubing (P/N 10010), an RTX-5 column (P/N 10208, cut to 5 m in length), and an Rt-Q-BOND column (P/N 19765, cut to 3 m in length) all with 250 μm inner diameter were purchased from Restek (Bellefonte, PA). A ShinCarbon ST micropacked column (P/N 19808) was also purchased from Restek. N-type silicon wafers (P/N 1095, 100 mm diameter, 500 μm thickness) and Borofloat 33 glass (P/N 517) were purchased from University Wafer. All materials were used as purchased without further purification or modification. Ultra-high purity 5.0 grade helium (P/N UN1046) was used as the auxiliary gas for the μHDPID and was purchased from PurityPlus (Indianapolis, Indiana).

3. Device fabrication

The μHDPID fabrication process is shown in Fig. 1(A). The μHDPID pattern is provided in the schematic shown in Fig. 1(B) and each individual section (*e.g.* plasma collection chamber, collection electrodes, auxiliary and analyte flow inlets, etc.) is labeled. A 175 μm thick Borofloat 33 glass wafer was bonded to a 400 μm thick silicon wafer at 330 °C under vacuum in order to reduce wafer bowing from thermal stress. Subsequently, 100 Å Cr followed by 5000 Å Au were deposited on a fresh 175 μm thick Borofloat 33 glass wafer and Si side of the bonded wafer. The two wafers were patterned with standard lithography processes with mirrored patterns and the Au and Cr were subsequently etched. The Si was then etched away completely (400 μm in depth) using deep reactive ion etching (DRIE) to form the fluidic chamber and channels. The photoresist was stripped from both wafers and the gold sides were bonded via eutectic bonding at 425 °C. A photograph of a single μHDPID chip is provided in Fig. 1(C). The final chip was 10 mm × 7 mm × 0.75 mm (L x W x H) in size. Additional chip dimensions are provided in Figure S1.

After dicing the chips, fluidic connections were formed by inserting guard columns into the inlet and outlet and sealing with Hysol® epoxy. Two pairs of electrodes were made for plasma generation and electrical readout by depositing MG Chemicals silver conductive epoxy on the top and bottom glass surfaces of the plasma chamber and the silicon readout electrodes, respectively. Wires were attached to these electrodes also using MG Chemicals silver conductive epoxy. The μHDPID was flushed with acetone and baked out at 200 °C for 1 h prior to use. Although plasma excitation electrodes could be deposited during microfabrication, no difference in performance was observed between the microfabricated electrodes and the epoxy electrodes. While solder offers some improvement in mechanical robustness, deposition of appropriate metal pads for wire soldering (instead of silver epoxy) would require additional microfabrication steps, since solder cannot easily adhere to silicon or Pyrex glass.

4. Device and circuit configuration

Due to the μHDPID's applicability to portable gas sensing, a small-scale circuit was developed in-house to accompany the μHDPID's small footprint. The circuit generates a stabilized high-voltage AC signal

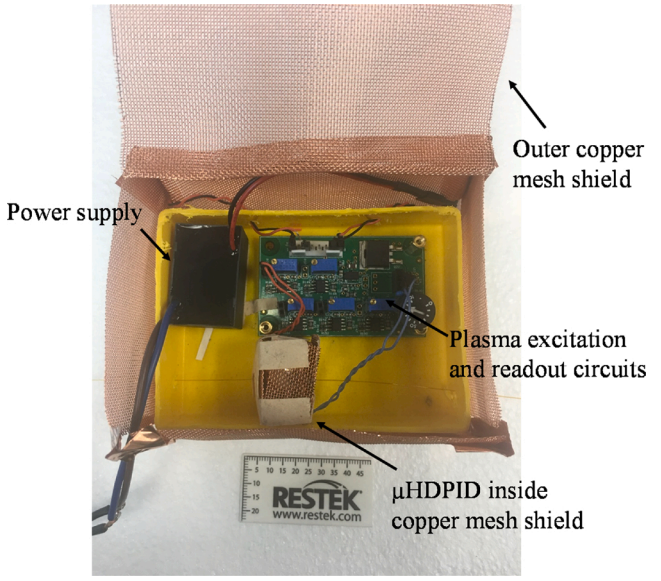

Fig. 3. Photograph of the μHDPID system, including power supply, plasma excitation and readout circuits, and μHDPID. The entire system size is 11.5 cm × 9cm × 5 cm and weighs 141 g.

of about 0.9 kV with a frequency of 83.6 kHz for plasma generation. This circuit (Fig. 2(A)) was designed using a NE555 astable multivibrator coupled with a step up transformer (ZS1052(H), Excelitas Technologies) through an n-channel MOSFET (IRF740SPBF). On the readout side, a bias voltage of 24 V was applied to the collection electrodes, where the current was then recorded by reading out a voltage drop across an external resistance circuit equivalent to ~102 MΩ. The voltage drop was further amplified using an INA122UA amplifier circuit, as shown in Fig. 2(B). A low pass filter with a cutoff frequency of 1.5 Hz was applied to the output of the amplification circuit. Notably, the supply voltage to the entire circuit was only 24 VDC, allowing for integration into low voltage, battery-operated portable systems. The total circuit cost was around only ~$250 (including both excitation and readout) and can be further reduced in the future with mass production ($100 – $150).

The total system power consumption was measured to be 1.2 W, the majority of which was consumed by the transformer circuit as heating (note that using an unbranded transformer purchased from eBay, the power consumption can be reduced down to ~393 mW with no loss in performance). The auxiliary helium flow rate was set to 10.5 mL/min for improved device performance, although the μHDPID can be operated with auxiliary flows as low as 5.2 mL/min. The entire device (including circuit and power supply) is contained within a copper shielding mesh of dimensions 11.5 cm × 9 cm × 5 cm, weighing 141 g (Fig. 3).

5. Experimental

The μHDPID was evaluated on all separations using an Agilent 6890 benchtop GC equipped with a split/splitless injection port. Manual injections of analytes were made using the injection port and separated using either a 5 m RTX-5 column (pentane, heptane, benzene, toluene, pyridine, tetrahydrofuran, ethyl acetate, acetone, isopropanol), 3 m Rt-Q-BOND column (dichloromethane, chloroform, carbon tetrachloride, methanol, formic acid, formaldehyde solution, acetaldehyde, water), 1 m deactivated fused silica capillary (oxygen, argon, carbon dioxide, methane, ethane, hydrogen, nitrogen), or ShinCarbon ST micropacked column (permanent gas mixture). All analytes were separated under isothermal conditions unless otherwise stated. The temperature was controlled by the GC oven. Ultra-high purity 5.0 grade helium was used as the carrier gas.

Table 1
μHDPID detection limits (DL) of various VOCs taken at 3σ, with σ =0.304 mV. Detection limits were calculated as averages based on 5 measurements. Ionization potentials (IPs) and injection amounts (IAs) are also reported for convenience. * compounds cannot be detected with regular 10.6 eV krypton lamps. Water cannot be detected with an 11.7 eV argon lamp.

Compound	DL (pg)	IA (pg)	IP (eV)
Toluene	5.1	513	8.82
Benzene	5.9	513	9.25
Pyridine	6.8	1163	9.32
Tetrahydrofuran	6.5	526	9.54
Acetone	6.5	464	9.69
Heptane	9.0	405	10.08
Ethyl acetate	6.1	534	10.11
Isopropanol	9.9	465	10.12
Acetaldehyde	6.4	467	10.21
Pentane	8.9	556	10.35
Methanol*	11.2	469	10.85
Formaldehyde*	13.4	476	10.87
Formic acid*	13.4	361	11.05
Dichloromethane*	12.3	525	11.35
Chloroform*	12.3	441	11.37
Carbon tetrachloride*	14.2	471	11.47
Water*	11.5	592	12.59

6. Results and discussion

6.1. Warm-up and response time

For a portable device, both the warm-up time and the response time are important parameters to ensure rapid responses to injected samples. The warm-up time was estimated by repeated injections of pure nitrogen directly after μHDPID plasma ignition (see Figure S2 for sample chromatogram). No peaks were observed within the first 10 s of plasma ignition. However, the first peak could be observed within 15 s after plasma ignition (Figure S2), demonstrating the μHDPID's rapid startup time.

The response time (defined as time taken for signal to rise from 10 % of peak height to 90 % of peak height) was estimated by repeated injections of methane into the μHDPID at a helium flow rate of 1.5 mL/min. Using a sampling rate of 4 Hz, the response time was estimated to be ~320 ms (average of 5 repetitions). However, if the sampling rate was increased to 200 Hz, the response time could be reduced to ~98 ms at the cost of a three times increase in noise (from 0.304 mV to 0.898 mV, 1σ). This response time is less than half of other reported micro HDPIDs (about ~200 – 400 ms) [21,23,25], demonstrating the capability for rapid responses suitable for fast GC. A sample overlay of the μHDPID methane responses with a FID methane response is provided in Figure S3.

6.2. Detection limit characterization

In order to characterize the μHDPID's ability to accurately detect low concentration samples, the detection limits of 17 compounds of varying ionization potentials were obtained (Table 1). Example separations of nitrogen, heptane, methane, and formaldehyde are shown in Figure S4. Detection limits were obtained by first calculating the signal to noise ratio (SNR) of peaks obtained from injection masses ranging from 360 to 600 pg (except for pyridine, injection mass was 1163 pg). The noise was calculated based on averaging the standard deviation noise (1σ) of ten 3 s segments of baseline signal, yielding σ =0.304 mV. Detection limits were calculated by dividing injection masses by corresponding SNRs (3σ noise level).

Table 1 shows that compounds with ionization potentials above 10.6 eV (or even 11.7 eV in the case of water) can be detected with detection limits close to ~10 pg. Detection limits below 10 pg can also be achieved for compounds with lower ionization potentials, such as pentane or benzene. The low detection limit is facilitated by two factors in the

Table 2
μHDPID detection limits (DL) of various gases taken at 3σ, with σ =0.304 mV. Detection limits were calculated as averages based on 5 measurements. Ionization potentials (IPs) and injection amounts (IAs) are also reported for convenience.

Gas	DL (pg)	IA (pg)	IP (eV)
Ethane	11.3	200	11.65
Oxygen	11.3	7000	12.08
Methane	11.8	3000	12.98
Carbon dioxide	14.7	10000	13.79
Hydrogen	18.8	3600	15.43
Nitrogen	18.5	3500	15.58
Argon	19.8	8500	15.76

μHDPID design. As compared with the previous HDPID [21], the plasma chamber volume is increased in the new design, meaning that helium ions are not as likely to be injected into the collection channel. In the original design, the plasma was generated inside a volume with a circular cross-sectional area 380 μm in diameter, resulting in high auxiliary flow speeds of over 100 cm/s. This created a plasma jet that could easily flow over into the collection electrodes, thereby increasing noise. The new increased plasma chamber volume greatly reduces the auxiliary flow to less than 1 cm/s at the boundary between plasma generation and analyte flow, which is nearly negligible compared to the carrier gas flow speed from the analyte side. Additionally, a silicon wall was added between the plasma discharge chamber and the collection electrodes (see Fig. 1(B)), acting as an ion and arc shutter to further reduce the amount of helium ions that could potentially be injected into the collection side. In combination with circuit optimization, these allowed for lowering of the μHDPID noise level and improvement of the detection limit.

6.3. Detection of light hydrocarbons and permanent gases

To further demonstrate the μHDPID's capability to serve as a universal detector for gas analysis, light hydrocarbons and permanent gases were injected and their detection limits were calculated (Table 2). Despite argon's high ionization potential (15.76 eV), the μHDPID was still capable of detecting it with a detection limit of better than 20 pg, considering the injection volume of 1 μL at a split ratio of 209:1 (concentration 1.784 g/L). The same was true for all other permanent gases and light hydrocarbons. A sample pulse response is provided in Figures S4(A) and (C), demonstrating a strong response with a 3.5 ng injection of pure nitrogen and 3 ng of pure methane.

6.4. Linearity

In Fig. 4, device linearity was examined for nine compounds of varying ionization potentials, with injection masses ranging from 50 pg to 10 ng for each compound. Highly linear responses were observed over the entire range, corroborating previously obtained results for the hand-assembled HDPID. Notably, the μHDPID was not adversely affected by injections of large amounts of moisture (methanol and water, up to 10 ng), suggesting that vapor condensation is not an issue in the present design. A linear dynamic range of ~4 orders of magnitude was observed for all nine compounds.

6.5. Repeatability between devices

The main advantage of the μHDPID is the robust microfabrication process, allowing for high repeatability among different devices. To examine this, the detection limits of heptane, benzene, dichloromethane, and nitrogen were examined for five different devices (5 repeated injections at each data point). Fig. 5 shows that the standard deviation of the detection limits for the five devices are 0.35 (3.9 %), 0.54 (8.4 %), 1.36 (10.6 %), and 0.38 (2.0 %) pg for heptane, benzene, dichloromethane, and nitrogen respectively. Values in percentages are calculated as deviation divided by the average of the detection limits of the five devices. The maximum deviation observed was 2.6 pg, or 20.3 % for dichloromethane, while on average, the deviation between devices was only 6.2 % (calculated as the average of the standard deviations divided by their respective detection limits). Notably, these results were

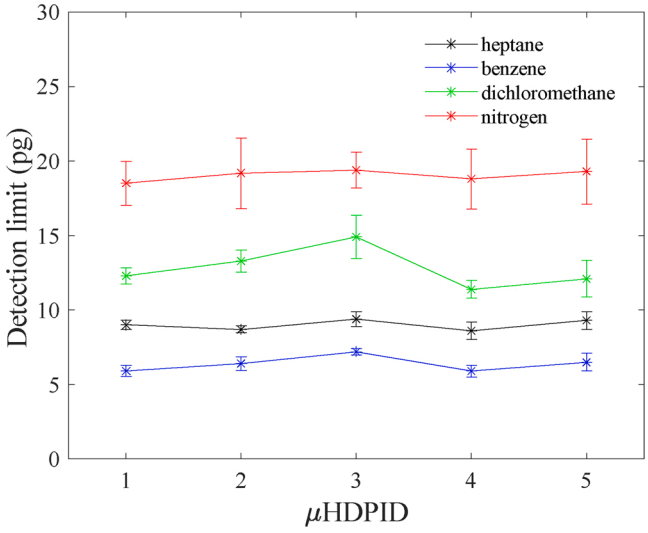

Fig. 5. μHDPID repeatability. The detection limits of heptane, benzene, dichloromethane, and nitrogen were measured (5 repeated injections for each data point) for 5 different devices. The detection limit variation between devices was no larger than 2.6 pg, or 20.3 % for dichloromethane.

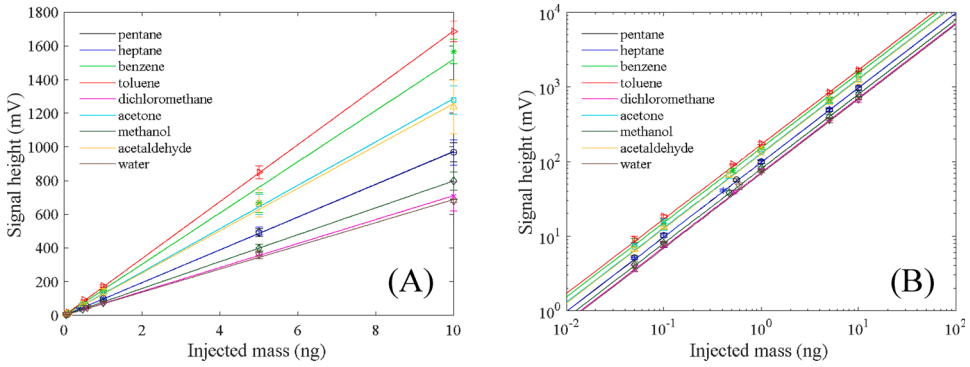

Fig. 4. μHDPID linearity on nine compounds with injection masses ranging from 50 pg to 10 ng. (A) Signal heights vs. injected masses plotted in linear-linear scale. (B) Signal heights vs. injected masses plotted in log-log scale. Error bars are obtained from five measurements. The R^2 values for the nine linear fits are 0.9999, 0.9996, 0.9945, 1.0000, 0.9996, 0.9997, 1.0000, 0.9985, and 0.9990 from pentane to water, respectively.

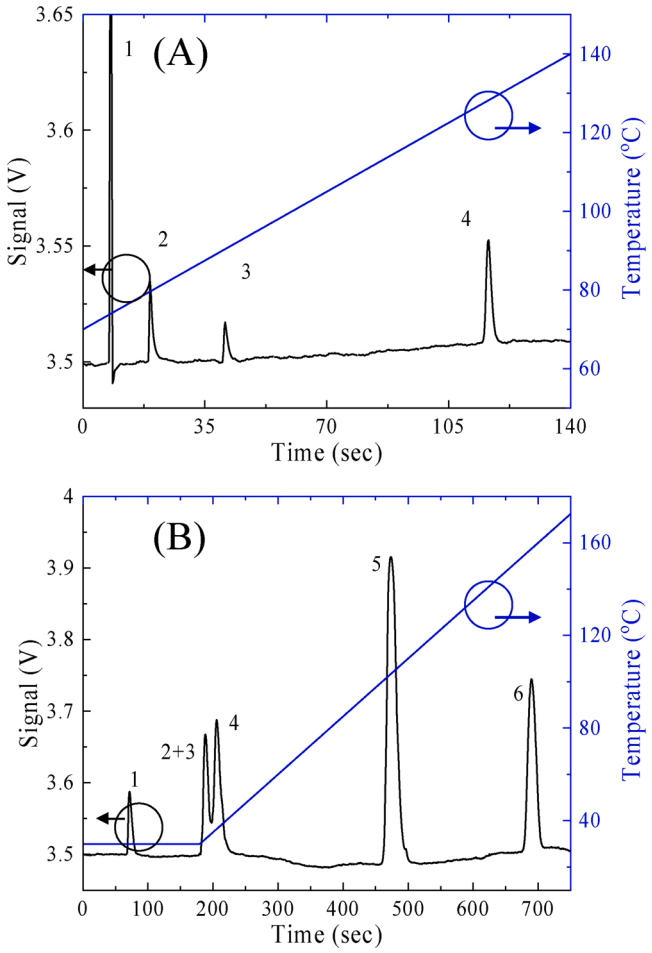

Fig. 6. (A) Separation of formaldehyde solution (methanol, water, and formaldehyde) using a 3 m Rt-Q-BOND column. An injection of 3 μL of headspace from the solution was made at a split ratio of 20:1 using a carrier gas flow rate of 3 mL/min at 70 °C. 1. Air; 2. Methanol; 3. Water; 4. Formaldehyde. (B) Separation of permanent gases using a ShinCarbon ST micropacked column. An injection of 50 μL of gas mixture was made using a carrier gas flow rate of 6.5 mL/min at 30 °C with a split ratio of 20:1. 1. Hydrogen; 2. Oxygen; 3. Argon; 4. Nitrogen; 5. Methane; 6. Carbon dioxide.

obtained using the same operating parameters for all devices (i.e., auxiliary flow rate, carrier gas flow rate, plasma excitation voltage, readout electrode bias voltage), demonstrating low inter-device variance. Further improvements to repeatability would involve more robust methods for electrode formation, such as deposition of gold-tin electrodes during microfabrication (for both readout electrodes and plasma generation) and soldering shorter, fixed-length wire interconnections.

6.6. GC chromatograms

In order to demonstrate the μHDPID's applicability to GC detection, two separations of formaldehyde solution and permanent gases were performed. The formaldehyde solution—consisting of methanol, water, and formaldehyde—was separated using a 3 m Rt-Q-BOND column with a temperature ramping profile of 70 °C ramped to 145 °C at a rate of 30 °C/min. The flow rate was 3 mL/min and the split ratio was 20:1. The resulting chromatogram is shown in Fig. 6(A) and demonstrates sharp peaks with peak widths (at half height) close to ~1−2 s.

A mixture of hydrogen, oxygen, argon, nitrogen, methane, and carbon dioxide was prepared for the permanent gas separation. This mixture was separated using a ShinCarbon ST micropacked column using a temperature ramping profile of 30 °C held for 3 min, then ramped to 180 °C at a rate of 15 °C/min. The flow rate was set to 6.5 mL/min and the split ratio was set to 20:1. Five of the six permanent gases were separated by the column (Fig. 6(B)), with oxygen and argon coeluted as the second peak. This separation confirms the μHDPID's capability to detect high ionization potential permanent gases.

7. Conclusion

The development and fabrication of an integrated μHDPID along with in-house plasma excitation and readout circuits has been detailed herein. The entire detector system was shown to be contained within a copper mesh of dimensions 11.5 cm × 9 cm × 5 cm, and only weighing 141 g. Analysis of permanent gases, light hydrocarbons, and formaldehyde was performed, demonstrating detection limits less than 10 pg for various volatile compounds and less than 20 pg for even high ionization energy permanent gases. High linearity for injections ranging from 50 pg to 10 ng was also observed, along with low warm-up time (within 15 s), and high repeatability between devices. Compared to the prior HDPID, the current μHDPID design offers the greatest advantages in ease of fabrication, fabrication yield and robustness, and repeatability. This on-chip, integrated fabrication allows for large-scale production of high quality μHDPIDs, which can be produced in bulk and used alongside or replacing the current lamp-based PID (ionization up to 11.7 eV) technology commonly used in portable GC systems. Furthermore, the low cost in-house developed circuits allow for reduction of the system size and operating voltage, improving the detector's overall portability. We anticipate that this μHDPID will significantly broaden the applicability of portable GC systems for detection of compounds with high ionization potentials such as hydrogen, methane, formaldehyde, other light hydrocarbons, and permanent gases.

CRediT authorship contribution statement

Maxwell Wei-Hao Li: Conceptualization, Data curation, Formal analysis, Investigation, Methodology, Writing - original draft, Writing - review & editing. **Abhishek Ghosh:** Methodology, Investigation, Writing - original draft. **Ruchi Sharma:** Methodology. **Hongbo Zhu:** Conceptualization. **Xudong Fan:** Conceptualization, Formal analysis, Resources, Supervision, Writing - review & editing.

Declaration of Competing Interest

The authors declare the following competing financial interest(s): Xudong Fan and Hongbo Zhu are the inventors of the HDPID described in the paper, which has been licensed to a company for commercialization.

Acknowledgments

The authors acknowledge support from NIOSH under grant R01 OH011082-01A1 and microfabrication aid from the Lurie Nanofabrication Facility at the University of Michigan.

Appendix A. Supplementary data

Supplementary material related to this article can be found, in the online version, at doi:https://doi.org/10.1016/j.snb.2021.129504.

References

[1] A.N. Freedman, The photoionization detector: theory, performance and application as a low-level monitor of oil vapour, J. Chromatogr. A 190 (1980) 263–273.
[2] J.N. Driscoll, M. Duffy, Photoionization detector: a versatile tool for environmental analysis, Chromatography 2 (1987).
[3] P. Verner, Photoionization detection and its application in gas chromatography, J. Chromatogr. A 300 (1984) 249–264.

[4] S. Narayanan, G. Rice, M. Agah, A micro-discharge photoionization detector for micro-gas chromatography, Microchim. Ichnoanal. Acta 181 (2013) 493–499.
[5] G. Coelho Rezende, S. Le Calvé, J.J. Brandner, D. Newport, Micro photoionization detectors, Sens. Actuators B: Chem. 287 (2019) 86–94.
[6] H. Zhu, R. Nidetz, M. Zhou, J. Lee, S. Buggaveeti, K. Kurabayashi, et al., Flow-through microfluidic photoionization detectors for rapid and highly sensitive vapor detection, Lab Chip 15 (2015) 3021–3029.
[7] J.C. Soo, E.G. Lee, R.F. LeBouf, M.L. Kashon, W. Chisholm, M. Harper, Evaluation of a portable gas chromatograph with photoionization detector under variations of VOC concentration, temperature, and relative humidity, J. Occup. Environ. Hyg. 15 (2018) 351–360.
[8] J.G.W. Price, D.C. Fenimore, P.G. Simmonds, A. Zlatkis, Design and operation of a photoionization detector for gas chromatography, Anal. Chem. 40 (2002) 541–547.
[9] W.-q. Zhang, H. Li, Y.-j. Zhang, F. Bi, L.-s. Meng, X.-m. Zhang, et al., Fast determination of monocyclic aromatic hydrocarbons in ambient air using a portable gas chromatography–photoionization detector, Chromatographia 80 (2017) 1233–1247.
[10] J. Lee, M. Zhou, H. Zhu, R. Nidetz, K. Kurabayashi, X. Fan, In situ calibration of micro-photoionization detectors in a multi-dimensional micro-gas chromatography system, Analyst 141 (2016) 4100–4107.
[11] D.-W. You, Y.-S. Seon, Y. Jang, J. Bang, J.-S. Oh, K.-W. Jung, A portable gas chromatograph for real-time monitoring of aromatic volatile organic compounds in air samples, J. Chromatogr. A 1625 (2020), 461267.
[12] S. Mendonca, W. Wentworth, E.C.M. Chen, S.D. Stearns, Relative responses of various classes of compounds using a pulsed discharge helium photoionization detector - experimental determination and theoretical calculations, J. Chromatogr. A 749 (1996) 131–148.
[13] W.E. Wentworth, H.M. Cai, S. Stearns, Pulsed discharge helium ionization detector universal detector for inorganic and organic-compounds at the low picogram level, J. Chromatogr. A 688 (1994) 135–152.
[14] R.R. Freeman, W.E. Wentworth, Helium photoionization detector utilizing a microwave discharge source, Anal. Chem. 43 (1971), 1987-+.
[15] Q.H. Jin, W.J. Yang, A.M. Yu, X.D. Tian, F.D. Wang, Helium direct current discharge ionization detector for gas chromatography, J. Chromatogr. A 761 (1997) 169–179.
[16] B.L. Winniford, K. Sun, J.F. Griffith, J.C. Luong, Universal and discriminative detection using a miniaturized pulsed discharge detector in comprehensive two-dimensional GC, J. Sep. Sci. 29 (2006) 2664–2670.
[17] J. Jalbert, R. Gilbert, P. Tetreault, Simultaneous determination of dissolved gases and moisture in mineral insulating oils by static headspace gas chromatography with helium photoionization pulsed discharge detection, Anal. Chem. 73 (2001) 3382–3391.
[18] H. Cai, S.D. Stearns, Pulsed discharge helium ionization detector with multiple combined bias/collecting electrodes for gas chromatography, J. Chromatogr. A 1284 (2013) 163–173.
[19] C.D. Mowry, A.S. Pimentel, E.S. Sparks, M.W. Moorman, K.E. Achyuthan, R. P. Manginell, Pulsed discharge helium ionization detector for highly sensitive aquametry, Anal. Sci. 32 (2016) 177–182.
[20] Y.B. Golubovskii, V.A. Maiorov, J. Behnke, J.F. Behnke, Modelling of the homogeneous barrier discharge in helium at atmospheric pressure, J. Phys. D Appl. Phys. 36 (2003) 39–49.
[21] H. Zhu, M. Zhou, J. Lee, R. Nidetz, K. Kurabayashi, X. Fan, Low-power miniaturized helium dielectric barrier discharge photoionization detectors for highly sensitive vapor detection, Anal. Chem. 88 (2016) 8780–8786.
[22] C.F. Poole, Ionization-based detectors for gas chromatography, J. Chromatogr. A 1421 (2015) 137–153.
[23] M. Akbar, H. Shakeel, M. Agah, GC-on-chip: integrated column and photoionization detector, Lab Chip 15 (2015) 1748–1758.
[24] J.G. Dojahn, W.E. Wentworth, S.N. Deming, S.D. Stearns, Determination of percent composition of a mixture analyzed by gas chromatography. Comparison of a helium pulsed-discharge photoionization detector with a flame ionization detector, J. Chromatogr. A 917 (2001) 187–204.
[25] S. Narayanan, G. Rice, M. Agah, Characterization of a micro-helium discharge detector for gas chromatography, Sens. Actuators B: Chem 206 (2015) 190–197.
[26] Y.M. Fu, S.C. Chu, C.J. Lu, Characteristic responses of an atmospheric pressure DC micro-plasma detector for gas chromatography to organic functional groups, Microchem. J. 89 (2008) 7–12.
[27] F.J. Andrade, J.T. Shelley, W.C. Wetzel, M.R. Webb, G. Gamez, S.J. Ray, et al., Atmospheric pressure chemical ionization source. 1. Ionization of compounds in the gas phase, Anal. Chem. 80 (2008) 2646–2653.
[28] J. Lasa, P. Mochalski, E. Lokas, L. Kedzior, Application of a pulse-discharge helium detector to the determination of neon in air and water, J. Chromatogr. A 968 (2002) 263–267.
[29] G. Gremaud, W.E. Wentworth, A. Zlatkis, R. Swatloski, E.C.M. Chen, S.D. Stearns, Windowless pulsed-discharge photoionization detector - application to qualitative analysis of volatile organic compounds, J. Chromatogr. A 724 (1996) 235–250.
[30] C. Meyer, S. Muller, E.L. Gurevich, J. Franzke, Dielectric barrier discharges in analytical chemistry, Analyst 136 (2011) 2427–2440.
[31] B. Han, X. Jiang, X. Hou, C. Zheng, Dielectric barrier discharge carbon atomic emission spectrometer: universal GC detector for volatile carbon-containing compounds, Anal. Chem. 86 (2014) 936–942.
[32] M.T. Jafari, Low-temperature plasma ionization ion mobility spectrometry, Anal. Chem. 83 (2011) 797–803.
[33] A. Bogaerts, E. Neyts, R. Gijbels, J. van der Mullen, Gas discharge plasmas and their applications, Spectrochimica Acta Part B 57 (2002) 609–658.
[34] R. Gras, J. Luong, M. Monagle, B. Winniford, Gas chromatographic applications with the dielectric barrier discharge detector, J. Chromatogr. Sci. 44 (2006) 101–107.
[35] K. Shinada, S. Horiike, S. Uchiyama, R. Takechi, T. Nishimoto, Development of new ionization detector for gas chromatography by applying dielectric barrier discharge. Shimadzu Review, 2012.
[36] D.S. Forsyth, Pulsed discharge detector: theory and applications, J. Chromatogr. A 1050 (2004) 63–68.

Maxwell Li obtained a B.E. and M.E. from the Univeristy of Michigan in 2017 and 2019 and is currently pursuing a Ph.D. in Electrical Engineering also at the University of Michigan. His current research includes micro/nano-fluidics, gas sensors, micro-fabrication, chemical analysis, and portable gas chromatography.

Abhishek Ghosh received his Ph.D. degree in Materials Science from Indian Institute of Technology, Kharagpur, India in 2018 and M.Tech in Material Science from National Institute of Technology, Durgapur, India in 2011. He is a former postdoctoral fellow at the University of North Texas, USA and presently working as a postdoctoral research associate at the department of Biomedical Engineering, University of Michigan, USA. His research includes metal oxide gas sensors, SAW gas sensors, air quality monitoring, PID sensors, and micro-gas chromatography.

Ruchi Sharma obtained B.Tech. in Electronics and Communication Engineering from NERIST, India, in the year 2005. She obtained M.Tech. in VLSI from Banasthali Vidyapith, India, in the year 2008, and Ph.D. in MEMS and Microelecorincs from IIT Delhi, India, in 2014. She joined the Biomedical Engineering Department at the University of Michigan as a postdoctoral research fellow in 2017. Between 2014 and 2017, she was a postdoctoral fellow at the University of Roma Tre, Rome, Italy, for a year and later joined the Department of Computer Science and Engineering, Washington University at Saint Louis, Missouri, USA, for a year. Dr. Sharma was awarded a distinction in the doctoral research and FITT award for best industry relevant Ph.D. thesis of 2014 at IIT Delhi. Her research includes MEMS and micro-electronics, microfabrication, electronics system design, gas sensors, portable gas chromatography, and its application in health care.

Hongbo Zhu received B.S. from Xiamen University in 2012 and M.S. from the University of Nebraska – Lincoln in 2014, and Ph.D. from the University of Michigan in 2019.

Xudong Fan obtained B.S. and M.S. from Peking University in 1991 and 1994, and Ph.D. in physics and optics from Oregon Center for Optics atthe University of Oregon in 2000. Between 2000 and 2004, he was a project leader at 3 M Company. In August of 2004, he joined the Department of Biological Engineering at the University of Missouri as an assistant professor and was promoted to Associate Professor in 2009. In January of 2010, he joined the Biomedical Engineering Department at the University of Michigan and was promoted to Professor in 2014. Dr. Fan is a Fellow of OSA, SPIE, and Royal Society of Chemistry (RSC). His research includes photonic bio/chemical sensors, micro/nano-fluidics, gas sensors, portable gas chromatography, and nanophotonics for disease diagnostics and bio/chemical molecule analysis.